Characterization of the Indoor Magnetic Field for Applications in Localization and Mapping

Michael Angermann*, Martin Frassl*, Marek Doniec†, Brian J. Julian†‡, and Patrick Robertson*

***Abstract*—To improve our understanding of the indoor properties of the perturbed Earth's magnetic field, we have developed a methodology to obtain dense and spatially referenced samples of the magnetic vector field on the ground's surface and in the free space above. This methodology draws on the use of various tracking techniques (photometric, odometric, and motion capture) to accurately determine the pose of the magnetic sensor, which can be positioned manually by humans or autonomously by robots to acquire densely gridded sample datasets. We show that the indoor magnetic field exhibits a fine-grained and persistent micro-structure of perturbations in terms of its direction and intensity. Instead of being a hindrance to indoor navigation, we believe that the variations of the three vector components are sufficiently expressive to form re-recognizable features based on which accurate localization is possible. We provide experimental results using our methodology to map the magnetic field on the ground's surface in our indoor research facilities. With the use of a magnetometer and very little computation, these resulting maps can serve to compensate the perturbations and subsequently determine pose of a human or robot in dead reckoning applications.**

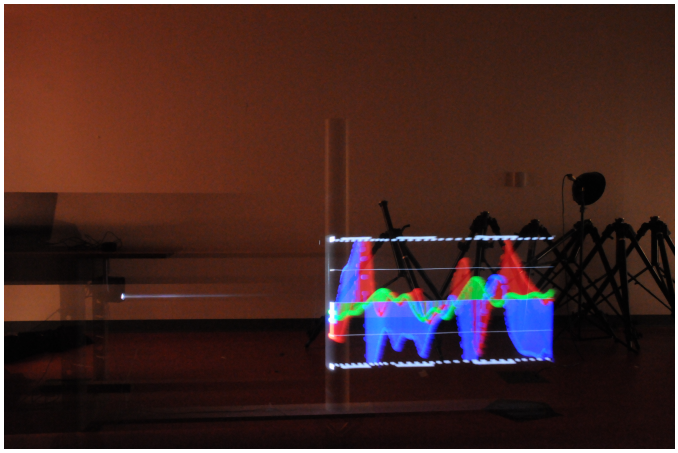

Fig. 1. An infrastructure-less photographic method achieves automatic spatial registration and visualization of one-dimensional magnetic field measurements. The projector and the cylindric projection surface are slightly visible.

I. Introduction

For millennia, humans have successfully employed the Earth's magnetic field for navigation. While a compass needle in combination with a map of magnetic declination is a simple and effective means to determine heading in outdoor locations, the Earth's magnetic field is generally believed to be of limited use in indoor environments due to strong perturbations caused by the abundance of ferromagnetic objects (e.g., pipes, ducts, rebar). In contrast, we believe the resulting omnipresent and information rich three-dimensional magnetic vector field can support not only heading estimates but also higher dimensional pose estimates in general.

A. Motivation

Sufficiently accurate indoor positioning is a key technology for a range of desirable professional and consumer applications and services. This technology would increase the safety of firefighters and law enforcement officers that greatly rely on their situational awareness; give more autonomy to industrial and personal robots that deliver goods and keep our houses clean; and enable commercial mass market applications that lead consumers to desired products or facilities. While good indoor localization has been achieved in robotics over the past two decades [1], these approaches are often based on odometry from proprioceptive sensors (e.g., wheel encoders) and environment features using active exteroceptive sensors (e.g., laser range finders). Indoor navigation for pedestrians has long been challenged by the lack of comparable and practical sensors for estimating motion and detecting features.

Recent work using foot-mounted inertial measurement units (IMUs) in combination with zero velocity updates has provided a feasible solution for obtaining pedestrian odometry [2]. However, the complimentary environment feature detection to prevent long-term inertial sensor drift remains an open research problem. Although approaches based on sensing persistent radio signals [3] or hitchhiking on human perception

*Michael Angermann, Martin Frassl, and Patrick Robertson are with the Institute of Communications and Navigation, German Aerospace Center (DLR), 82234 Wessling, Germany, firstname.lastname@dlr.de

†Marek Doniec and Brian J. Julian are with the Computer Science and Artificial Intelligence Laboratory, MIT, Cambridge, MA 02139, USA, doniec@mit.edu and bjulian@mit.edu

‡Brian J. Julian is also with MIT Lincoln Laboratory, 244 Wood Street, Lexington, MA 02420, USA

The authors would like to thank Oliver Heirich (DLR) for the initial Java wrapper to the sensor package and Alan Jennings (University of Dayton, Ohio) for the Matlab implementation of SphereFit used for the calibration. In addition, the authors would like to thank Daniela Rus (MIT) for her support and for the use of CSAIL's motion capture system.

This work is supported by the European Community's FP7 Programme (FP7/20072013) under Grant 2574943 of the Societies Project and by DLR under Project Dependable Navigation. In addition, the authors would like to thank the AUTOMATE Project at MIT Lincoln Laboratory for the use of the omnidirectional ground robot.

This work is sponsored by the Department of the Air Force under Air Force contract number FA8721-05-C-0002. The opinions, interpretations, recommendations, and conclusions are those of the authors and are not necessarily endorsed by the United States Government.

978-1-4673-1954-6/12/$31.00

[4], [5] have been proposed, they come at the price of a dedicated radio infrastructure, difficult propagation conditions, or significant computational cost. Since foot-mounted IMUs often have magnetic field vector sensing capabilities, it is unfortunate that the resulting signal of large spatial variation is usually considered to be of little use for heading correction. We reckon that these spatial variations provide very informative features that could be sensed at little computational cost. Thus, they provide the needed external reference for sufficient observability of inertial sensor drift in order to achieve long-term stable and highly accurate indoor navigation.

B. Problem Statement

We wish to study the properties of the magnetic vector field in static indoor environments, and in doing so consider this field to be constant in time and varying in direction and intensity over the three-dimensional free space surrounded by floors, walls or physical objects, such as furniture or machinery. We do not attempt to interpret the measured field in terms of the physical causes. We are particularly interested in the spatial spectral characteristics of the field, since these are related to bounds on accuracy for indoor localization. Furthermore, the signal-to-noise ratio of measurements of this field will have strong influence on how well it may be usable for localization purposes.

C. Related Work

We are inspired by the previous research that goes against common belief and uses the magnetic vector field for localization in indoor environments. Motivated by correcting for the long-term drifting of inertial turn rate sensors, many approaches detect spatial subsets of the indoor environment where the Earth's magnetic field is not greatly disturbed. Bird et al. [6] suspended magnetic heading calculations when anomalies in the magnetic field were identified, suggesting that "the effects of the external anomalies cannot be estimated." Similarly, Afzal et al. [7] proposed using a detector in combination with a fuzzy-logic based inference system to signal undisturbed heading estimates, thus isolating "the perturbed regions from the clean ones." While accurate heading estimates are also desirable for our work, we focus on employing rather than avoiding the disturbances of the magnetic field to help in localization.

For translational position determination in robotic and pedestrian navigation, magnetic field-based localization in indoor environments has only recently gained attention. Gozick et al. [8] discuss the creation of maps containing magnetic landmarks for indoor navigation using mobile phones embedded Hall sensors. They showed that such landmarks of increased magnetic intensities are the result of common indoor objects such as large pillars or vending machines. Gozick et al. provided field intensity datasets taken in the corridors at the University of North Texas and showed that the magnetic signatures were stable over a period of several months. In contrast to this work, we are interested in the variations of the field on a much finer scale, i.e., the order of centimeters instead of meters. We also make specific use of the vector-field nature of the magnetic field instead of using only its intensity.

Drawing on an analogy to terrain matching in navigation, Storms et al. [9] proposed to use the magnetic field and its location dependent features to aid an inertial navigation system in GNSS-denied environments. To our knowledge, they are among the first to recognize "that the variations of the magnetic field in indoor environments can be used as a way to identify a user's position, and possibly orientation, because the three-dimensional magnetic field varies significantly as a function of position." They showed the feasibility of a Kalman Filter-based approach by using a Honeywell HMR2300 magnetic sensor to first build a map then localize within that map at decimeter-level accuracy. Additionally, Storms et al. described a "leader-follower scenario" to enable a follower to accurately match a leader's motion trajectory using only magnetic measurements. This leader-follower concept was extended by Riehle et al. [10] to replay audio annotations at predefined locations along predefined indoor routes with the aim of assisting visually impaired individuals.

With respect to Simultaneous Localization and Mapping (SLAM), Vallivaara et al. showed that geometrically consistent maps can be produced from a magnetic field dataset [11]. They reported convergence in 19 out of 20 particle filter runs on a dataset acquired using an iRobot Create mobile robot platform equipped with a MicroMag 3-axis magnetometer positioned approximately 40 cm above the surface of the ground (judging by the published pictures). Vallivaara et al. also presented positioning errors with mean standard deviation of between 5 cm and 10 cm using the same platform and sensor [12]. The results of both works are particularly encouraging for our efforts, since we strive to bring the magnetic sensor as close to the ground as possible, which we expect to result in a higher spatial bandwidth and persistence of the field.

II. Indoor Magnetic Field Background

The geomagnetic field generated by the motion of molten iron alloys in the Earth's outer core is relatively undisturbed in most outdoor environments. A compass needle suffices to measure the horizontal direction of this field and estimate heading based on a very simple dipole model. The availability of correction charts for local inclination and declination further increases the accuracy of the heading estimate, and thus this simple approach has long been successfully utilized in sea, air and land navigation.

The fact that the disturbances of the outdoor field do not change quickly with location is advantageous in two ways. Firstly, the amount of information needed to map and correct for these disturbances is relatively small. For many applications, paper charts with local inclination and declination provide sufficient information to achieve desired heading accuracy. Secondly, the translational motion of a person or vehicle does not typically move the magnetic sensor at a rate where the orientation of the external field changes significantly. Hence, the available integration interval of the compass is only limited by the expected rotational dynamics of the sensor, which is

one of the reasons why a compass needle has been used so successfully despite its rotational inertia and the relatively little torque exerted by the Earth's magnetic field.

In contrast to the low spatial frequencies of the outdoor magnetic vector field, the indoor field may change on a scale of a few centimeters or less, as we will discuss below. The increased spatial frequency requires a far larger amount of information to correct for disturbances and requires much shorter integration intervals or higher filter bandwidths that are no longer dominated by the sensor's rotational dynamics but instead by its translational velocity. The relevance of our work is owed to the composition and omnipresence of reinforced concrete in modern building structures, such as floors, walls, beams or pillars. In these structures concrete, a mixture of stones, sand, and cement is combined with reinforcing steel ("rebar") as shown in Figs. 2(a) and 2(b).

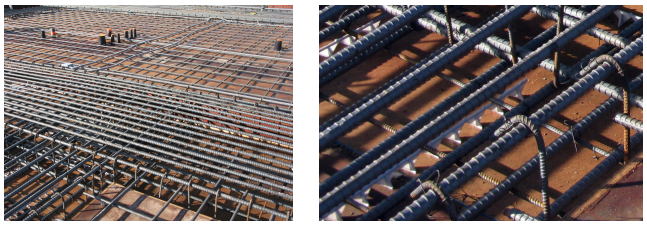

(a) rebar before pouring of concrete (b) detailed structure

Fig. 2. The geometry of reinforcing steel structures in modern building structures is intricate and creates complex distortions in the magnetic field. The spatial frequencies of these distortions are closely related to the geometry of the steel structures and generally in the same scale.

The details of the magnetic properties of steel are complex and beyond the scope of this paper. It suffices to observe that in most cases the presence of steel significantly distorts the local magnetic field. The distortion is a function of the geometry of the steel and decreases with distance to the steel structures. While steel structures are the dominant contributor to (static) distortions of the indoor magnetic field, other sources may include DC currents, permanent magnets or other metal objects with ferromagnetic properties. The following work does not distinguish between these sources. We also do not distinguish between the original field and the distortions, but instead describe the resulting field as one vector field $f_B : \mathbf{x} \in \mathbb{R}^3 \mapsto \mathbf{B} \in \mathbb{R}^3$, that maps every position $\mathbf{x} = [x, y, z]^T$ to a field vector with three orthogonal components $\mathbf{B} = [B_x, B_y, B_z]^T$. We assume that a sensor exists that is defined by its sensing function $f_s : \langle \mathbf{B} \in \mathbb{R}^3, \mathbf{r} \in \mathbb{R}^3 \rangle \mapsto \mathbf{z} \in \mathbb{R}^3$ that maps the field vector at the sensor's position and attitude $\mathbf{r} = [r_x, r_y, r_z]^T$ to a sensor reading $\mathbf{z} = [z_x, z_y, z_z]^T$.

For the purpose of this work we further assume the geomagnetic field to be stationary over time and neglect any short-term variations, such as geomagnetic storms caused by solar flares or secular variations (e.g., the slow changes of magnetic declination and intensity observable over time-scales of hundreds of years). In the following discussion we use the SI derived unit for the magnitude of the magnetic B-field, which is 1 tesla (T), with $\mathrm{T} = \mathrm{kg} \cdot \mathrm{A}^{-1} \cdot \mathrm{s}^{-2}$. The earth's magnetic field is often conveniently reported using the unit 1 gauss (G) of the CGS system, with $1\ \mathrm{G} = 0.0001\ \mathrm{T}$. On the Earth's surface the intensity of the geomagnetic field ranges approximately from 0.25 G to 0.65 G.

III. Experimental Setup

A. Sensor Hardware

The magnetic field sensor used in the reported experiments uses three orthogonal thin film magneto-resistive sensor units. This triad of sensors is part of a commercial integrated sensor package (xsens MTx). In addition to a magnetic sensor triad, this package contains accelerometer and gyrometer triads. The sensor communicates via USB using a proprietary protocol for configuration and data logging. For the experiments a sampling rate of 100 Hz has been used. According to its specification the sensor's bandwidth is 10 Hz. Nevertheless, the experimental results show that sensor is also sensitive at significantly higher frequencies.

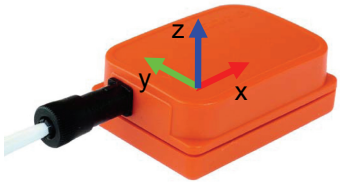

Fig. 3. Sensor package including three-axis magnetometer, accelerometer and gyroscope. The orientation of the axes of the body frame is shown.

B. Sensor Calibration

In an initial calibration phase prior to each of our experiments the sensor is manually rotated around all three axes as randomly and with as little translation as possible. The raw sensor output during this calibration phase is recorded and a sphere is least-squares fitted so that the three raw sensor outputs lie on the spheres surface. The coordinates of the center of fitted sphere are used as an estimate for the three biases. The radius of the sphere is used to normalize the measurements to the intensity of the geomagnetic field at the location of the experiment. Fig. 4 shows the result of a calibration phase in raw sensor units.

As an estimate of the actual intensity of the geomagnetic field we are using data reported by the Munich Earth Observatory. This observatory takes measurements at their Fürstenfeldbruck site (IAGA code FUR), less than 15 km from our DLR lab and has reported an average intensity of 48180.23 nT for July 2012 [14]. The radius of the least-squares estimated sphere fit to the sensor data shown in Fig. 4 is 7829 raw sensor units, resulting in a scaling factor of approximately 6.15 nT/raw sensor unit.

C. One-dimensional Photographic Method

Since human perception does not include a sense for magnetic fields, being able to convert the magnetic field to one of our sensing modalities with little effort would be helpful to improve our understanding of the properties of the magnetic

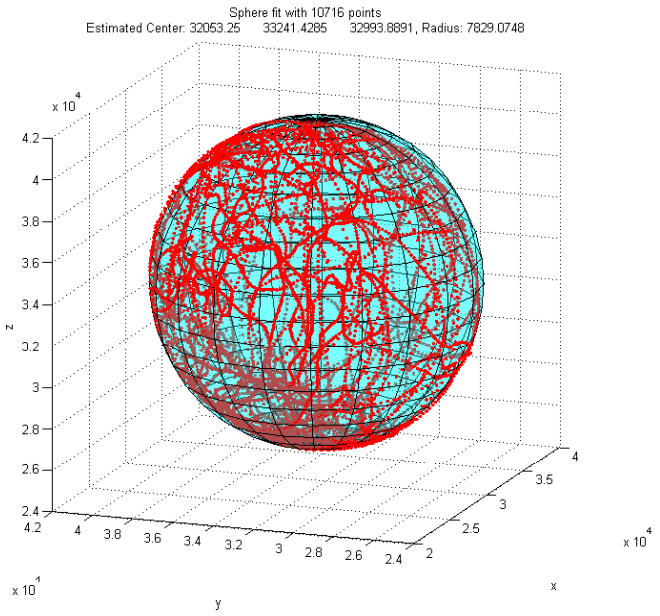

Fig. 4. For calibration the sensor is manually rotated with as little translation as possible. A sphere is fitted to the three raw sensor outputs. The raw sensor outputs are shown in red.

field. For this purpose, we have derived a method that allows to spatially register and visualize the components of the magnetic field. Moreover, the method requires no infrastructure and only few components, allowing for easy replication. In addition, we wish to sense the magnetic field while contributing as little additional disturbances as possible with the sensing apparatus. Thus, we position the actual sensor (as shown in Fig. 3) at the desired location while keeping all other electronic components a sufficient distance away. Fig. 5 illustrates the overall setup.

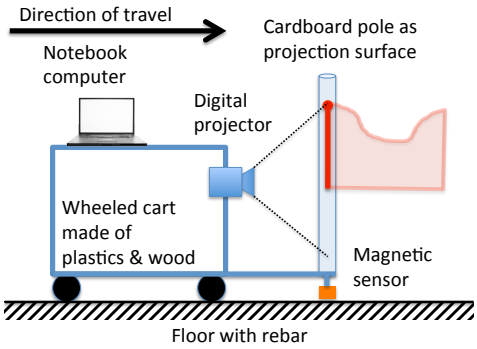

Fig. 5. Illustration of the setup for the one-dimensional photographic method.

The sensor package is mounted underneath a wooden beam that is fixed to a plastic pushcart. A vertically oriented white cylinder made of cardboard is mounted directly above the sensor package. This cylinder serves as a projection screen for a projector that is mounted on the pushcart. The sensor is connected to a notebook computer, also on the pushcart, that creates and displays a panel with three bars using a miniature projector. Each bar is a few pixel wide and its length corresponds to the intensity of one vector component of the sensed magnetic field. The three field components are separated using different colors. If the entire setup is moved along a trajectory, the changing field modulates the lengths of the bars displayed on the white cylinder. Fig. 1 shows how a photographic long term-exposure (e.g., 10 seconds for a 5 meter long trajectory at 0.5 m/s movement) creates a "floating" image of the magnetic field components that is inherently spatially registered.

D. One-dimensional Odometric Method

The photographic method is well suited for providing insight in settings were the camera perspective can be chosen to be orthogonal to the trajectory of the sensor. In order to obtain measurements along a corridor, where it is difficult to obtain this perspective, we maintain the principle of keeping the sensor package spatially separated from other electronics components. Instead of the inherent spatial registration we employ traditional wheel odometry. For better mobility, we have also replaced the pushcart with a flat sled. In the setup shown in concept and realization in Figs. 6 and 7 the sensor is mounted on an elongated sled made of acrylic that glides on the surface of the floor.

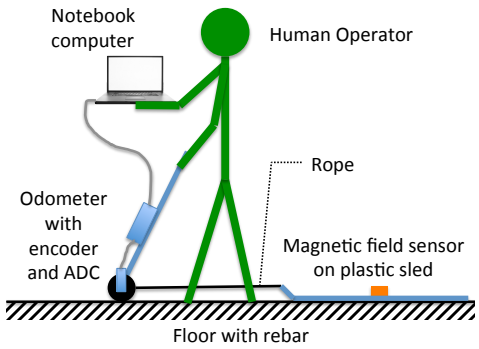

Fig. 6. Illustration of the setup for the one-dimensional odometric method.

The sled is dragged behind a handheld wheel odometer, which has been retrofitted with a high resolution wheel encoder. The quadrature signal of the wheel encoder is converted, timestamped, and recorded with a hand-carried notebook computer. All three magnetic field components are timestamped and recorded in parallel. The timestamps facilitate the analysis of the magnetic field in the time-domain as shown in Fig. 9 as well as spatial registration with the recorded odometry as shown in Fig. 12.

E. Two-dimensional Tracking Method

While the two previously described methods provide good insight into both the macro- and microscale of the magnetic field, they are not well-suited for higher-dimensional mapping of a field. In order to obtain high-resolution two dimensional maps of our indoor laboratories at DLR and MIT CSAIL, we use both manual positioning of the sensor as well as

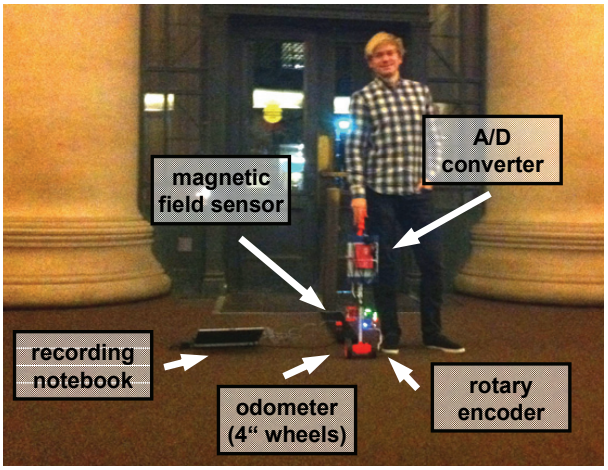

Fig. 7. Setup for one-dimensional odometric method. The sensor (orange) is mounted on an elongated sled made of 4 mm thick acrylic (PMMA) sheet material. The sled is dragged behind a wheeled odometer. The odometer is retrofitted with a wheel encoder. The quadrature signal of the wheel encoder is A/D-converted using a digital oscilloscope. All signals from the magnetic sensor and the wheel odometry are recorded with a notebook computer.

an omnidirectional ground robot in conjunction with optical motion tracking systems to control and record the ground-truth position of and readings from the magnetic sensor. For mapping of small areas ($< 1\,\mathrm{m}^2$) we use manual positioning in combination with a simple wooden fixture for moving the sensor along a rectangular grid with 1 cm spacing. While the fixture guides the movement, the actual ground truth position is recorded with an optical tracking system.

For mapping of wider areas with a ground robot, the magnetic sensor is suspended approximately 2 cm above the surface of the ground within a cardboard box. By attaching IR reflective spherical markers on the cardboard box at known positions, the motion capture system locates the magnetic sensor assembly within our indoor laboratory with millimeter accuracy. A meter long wooden beam cantilevers the magnetic sensor assembly from the platform of the ground robot. Using the realtime position feedback, a linear quadratic regulator controls the ground robot to position the magnetic sensor assembly within 2.5 mm (translational) and 100 mrad (rotational) from a desired location. We use this methodology to acquire a dense 5 cm square grid of samples over a 4 m by 2 m area in Section IV-B.

IV. Experimental Results

A. Large Scale One-dimensional Mapping

We have used the one-dimensional odometric setup described in section III-D to map the magnetic field inside of the “Infinite Corridor”, a 250 meter long hallway that runs through the main buildings of MIT. Fig. 9 shows the three components of the magnetic fields over the duration of one run, starting from Killian court and ending at Massachusetts Avenue. The setup was immobile for approximately 100 seconds and then manually driven towards the other end of the hallway.

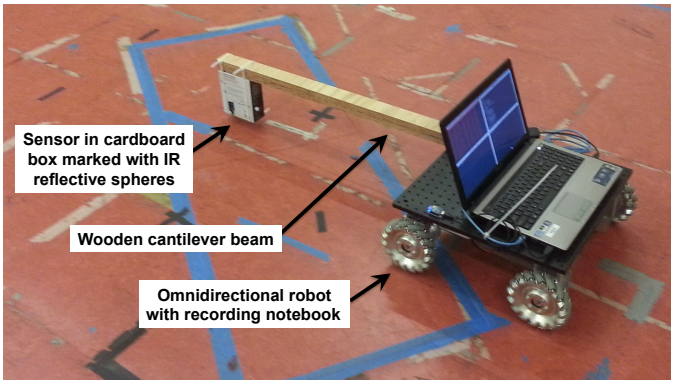

Fig. 8. A snapshot taken during our two-dimensional data collection.

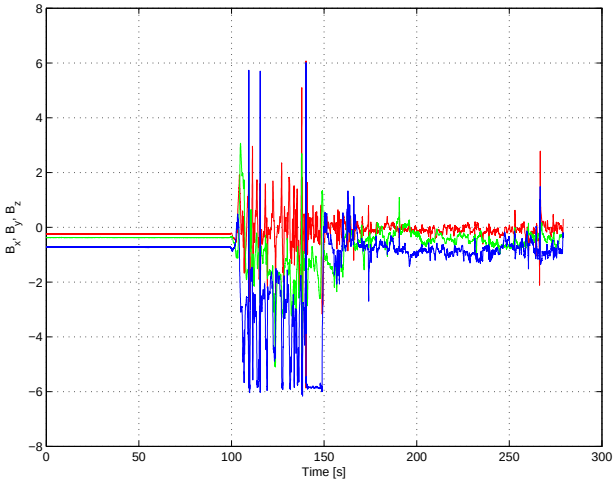

Fig. 9. Measurement of the three components of the magnetic field sampled at 100 Hz during a run of approximately 180 seconds.

Fig. 10 shows an initial spectral analysis of the data. Note that this analysis has been performed to see spectral components with relation to time, not to space, in order to see the influence of time-varying fields.

The spectral analysis shows an almost continuous presence of spectral components at 20 Hz and 40 Hz. These spectral components are explainable by the presence of 60 Hz AC currents in combination with sampling at 100 Hz, effectively violating the Nyquist–Shannon sampling theorem and leading to aliasing, if the signals are considered to be in baseband. Particularly strong fields seem to have occurred around 200 seconds and 240 seconds. Fig. 11 shows a closer look at the signal around 240 seconds in the time domain. The influence is clearly visible in the time domain.

A spatially registered map of the magnetic field is created by combined the wheel-based odometry and the measurements of the magnetic field based on their timestamps. Due to relatively constant speed during the run the temporal signal as shown if Fig. 9 and the spatially registered map as shown in Fig. 12 look very similar.

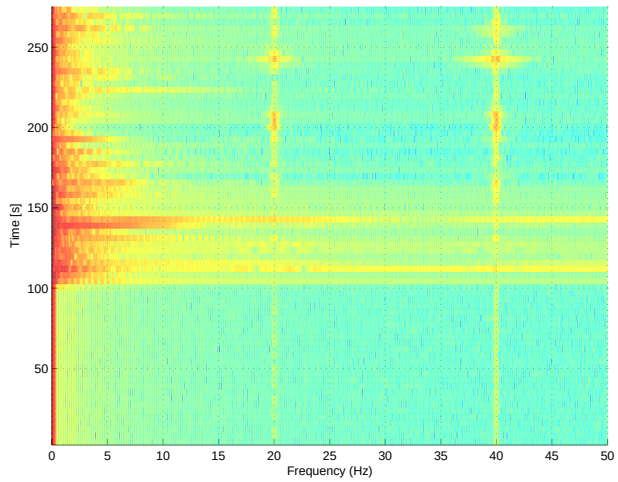

Fig. 10. Spectral analysis of the measurements (here B_y) shows 60 Hz AC currents in the environments at 20 Hz and 40 Hz due to aliasing (F_s =100 Hz). Apparently strong fields have been passed at 200 seconds and 240 seconds.

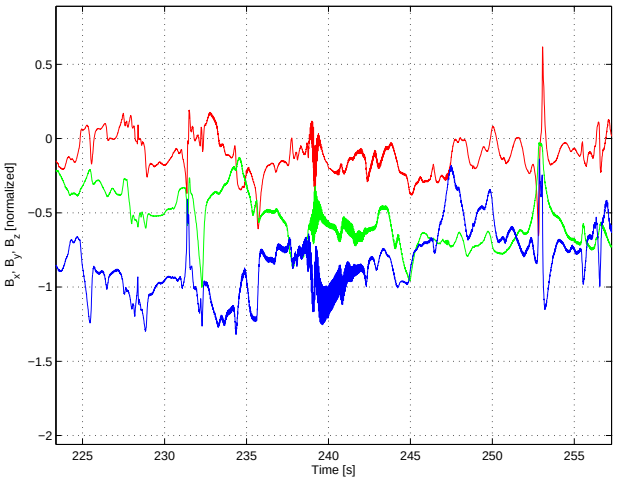

Fig. 11. The strong fields visible in the spectral domain are also visible in the temporal domain. Here the event at 240 seconds is shown in more detail.

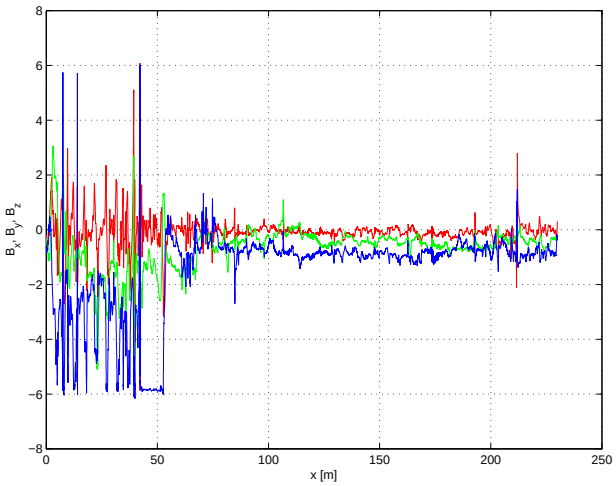

Fig. 12. Resulting map of spatially registered magnetic field components based on wheel odometry.

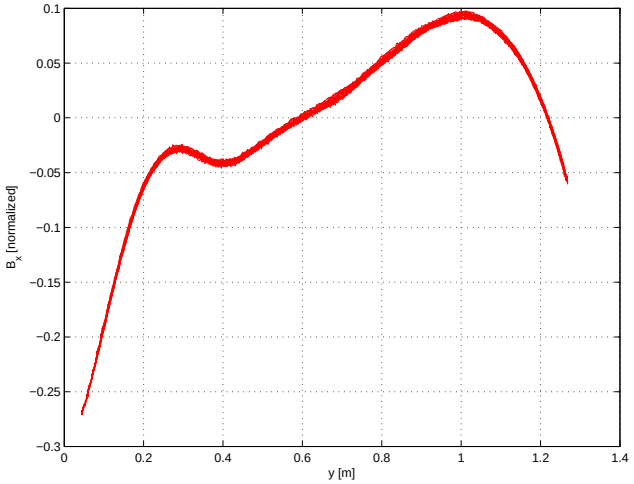

Fig. 13. Aggregate of 20 measurements of B_x over a line segment of approximately 1 m. The curve show relatively strong modulation and little noise.

B. Two-dimensional Mapping

Since the large scale measurements described in the previous section have shown very fine-grained structure, we wish to study the disturbances in one and two dimensions at the scale of the structures that cause them. We use the two-dimensional tracking method described in section III-E to generate high resolution maps of the magnetic field. In a first experiment in our laboratory at DLR in Oberpfaffenhofen, we manually moved (i.e., without the omnidirectional robot) the magnetic sensor 10 times back and forth over a line segment of approximately 1 m length. Fig. 13 shows the point cloud that results from effectively 20 passes at each position when plotting one component of the field (here B_x) over the position the measurement is taken at.

We see that the magnetic field is strongly modulated over this rather short distance and that the measurement is subject to relatively little noise. A zoom into a 5 cm wide segment is shown in Fig. 14. A comparison of the amount of noise with the modulation present in these few centimeters suggests good observability of location from the field measurements.

While the good signal-to-noise ratio is a prerequisite for accuracy, it is also relevant to consider in how far a single measurement is useable to directly infer the location or how much ambiguity is caused by a curve like the one in Fig. 13 being not strictly monotonic. Particularly helpful is the vector character of the magnetic field which effectively provides a total of three useable sensor functions at each sampling location. In Fig. 15 we can see that the diversity of the three field components may help in preventing or resolving

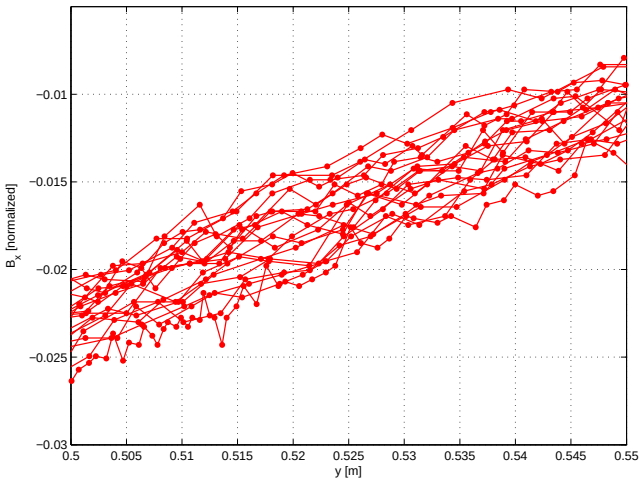

Fig. 14. A zoom shows the 20 individual measurement series on a 5 cm segment of the curve in Fig. 13 that suggests good observability of the position.

ambiguities.

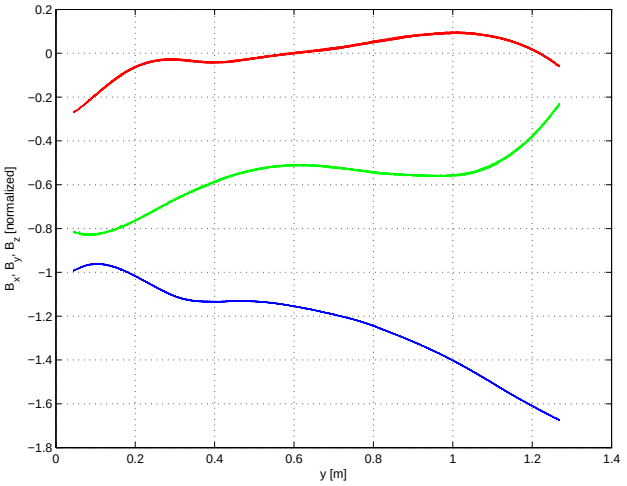

Fig. 15. Aggregate of 20 measurements of all three field components. The significantly distinct shapes hint good properties for resolving ambiguities in location.

Plotting the curve traced by the vector of the magnetic field provides insight into the ambiguities present in a specific line segment or area. The non-overlapping curve depicted in Fig. 16 shows that no ambiguity is present in the magnetic field on this particular line segment.

To investigate how accurate location may be determined based on a map of the field and a single vector-valued sample of the three field measurements, we have created a map by taking the mean of the 20 measurement series. We have then taken a single sample of the three vector components at a random location and have computed the Euclidean distance of the sample to each location's magnetic field vector stored in the map. In Fig. 17 the Euclidean distance is depicted for all

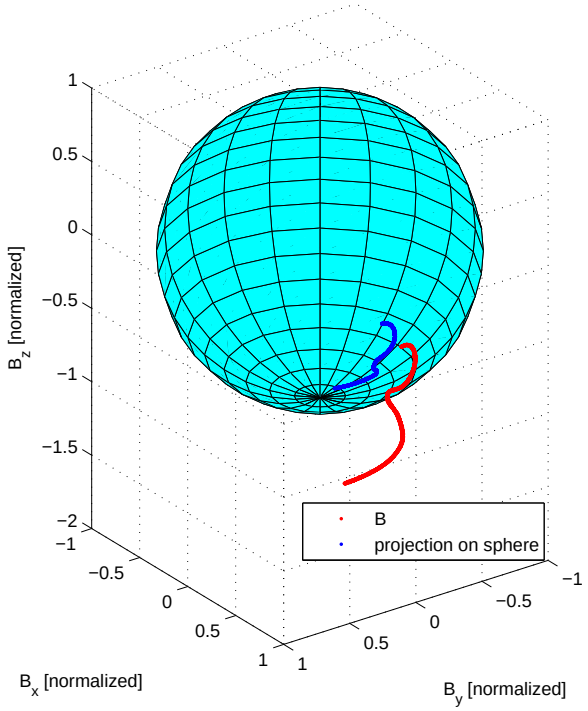

Fig. 16. The magnetic field vector formed by the three components traces a non-overlapping curve in space for the data shown in Fig. 15. This shows that on this segment the data is sufficiently informative to prevent any ambiguity.

candidate locations. We see that this distance has a distinct minimum and zooming into the location of this minimum shows that the location can be inferred with sub-centimeter accuracy from the single sample for this particular map and sample location.

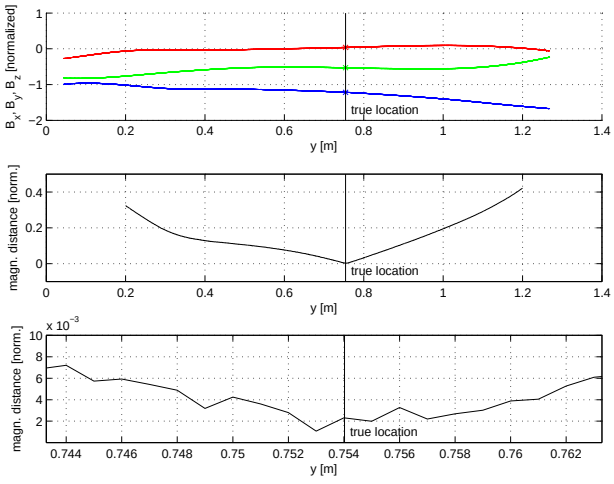

Fig. 17. The mean of the 20 measurement series is used as a map (top). One sample is taken at an arbitrary location. The Euclidian distance of this sample to all points on the map is plotted (middle). The zoom (bottom) shows that the location can be inferred with sub-centimeter accuracy.

We have then used manual positioning of the sensor to sample a dense two-dimensional map. We can see in Figs. 18 and 19 that in both dimensions the modulation is strong compared to the noise level.

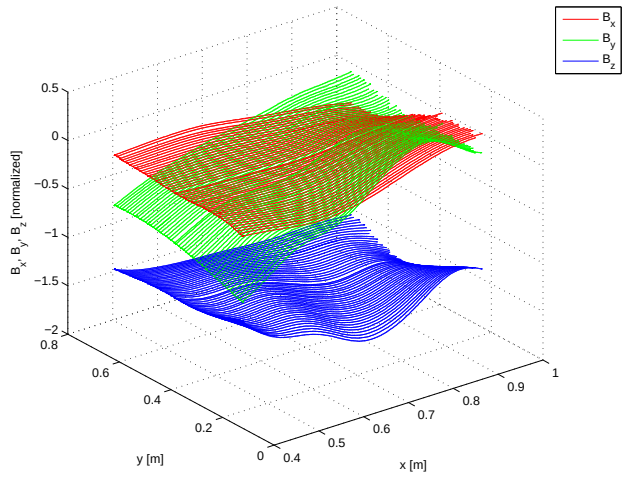

Fig. 18. Two-dimensional map of all three magnetic field components obtained with manual positioning of the sensor.

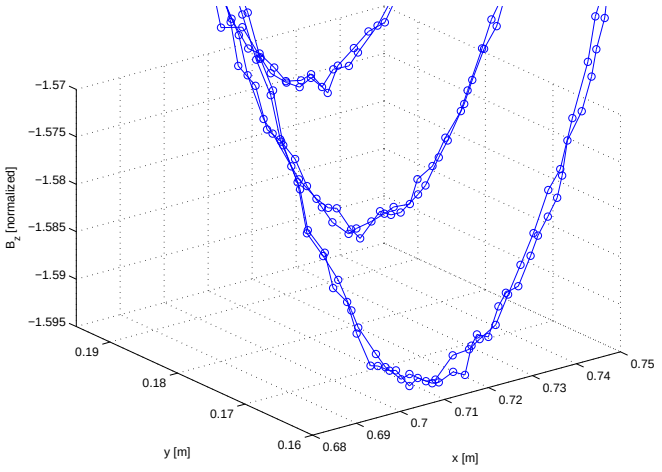

Fig. 19. A zoom into the 2D measurements shows that the back and forth passes of each line are fairly consistent. The noise in the magnetic field measurements is relatively small compared to the field's modulation along and across the lines. The lines are separated by approx. 1 cm.

A map of the intensity, i.e. the 2-norm of the magnetic field vector is depicted in Fig. 20 and also shows good signal-to-noise ratio. It is advantageous that the 2-norm allows to match in ignorance of the sensor's attitude. The downside of that property is that the 2-norm lacks to ability to observe or infer the orientation. Furthermore, it is also less capable to prevent or resolve ambiguities.

In order to obtain a first indication whether a resulting 2D map could be employed for localization purposes, we used the collected data to first create a grid-based magnetic map with a

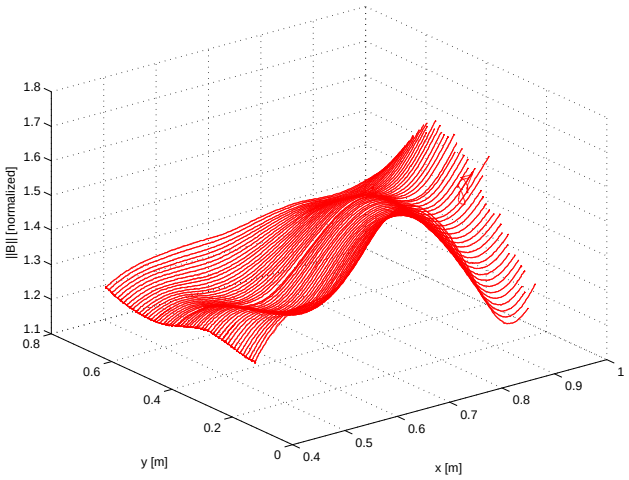

Fig. 20. The intensity of the magnetic field shows also little noise compared to the significant modulation.

spatial resolution of 10 cm. We then interpolated this map to a spatial resolution of 1 cm and used the resulting map to localize a trajectory of measurements using a particle filter with $N = 1000$ particles. Simulated sensor noise was added to the measurements. The standard deviation of the simulated noise was chosen to match the noise visible in the original data. We did not employ any odometric information. The prediction step randomly moved the particles with standard deviations of 1 cm in x and y. Particles were weighted according to their fit with the measurements and then resampled. The resulting trajectories are plotted in Figure 21.

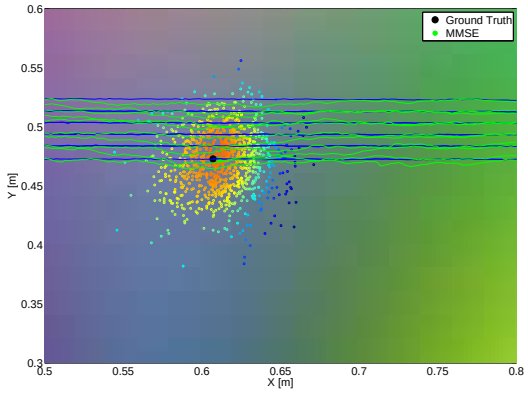

Fig. 21. Localization on small-scale with a particle filter. Blue lines denote ground-truth positions, green lines are the filter's minimum mean square error (MMSE) position estimates

The blue lines denote the ground-truth captured during data collection and the green lines are the particle filter's minimum mean square error (MMSE) position estimates.

74 % of the errors are 1 cm or less, which is the resolution of the magnetic map used for estimation. We note that these particular localization results should be taken with a grain of salt. Lacking additional data at the time this submission was

prepared, the measurements of the trajectory were among the ones that contributed to the map. While we are inclined to assume that the additional noise in combination with the two-step process of coarsely gridding and subsequently interpolating the map should prevent overfitting, we are fully aware that data for training (mapping) and data for testing (localizing) need to be separated to properly evaluate performance in future work.

We then used the omnidirectional robot described in III-E to create an interpolated two-dimensional map of B_x, B_y and B_z of a larger area (4 m by 2 m). As expected, we see in Fig. 22 that strong spatial modulation in both dimensions of the floor is visible in all three components of the field.

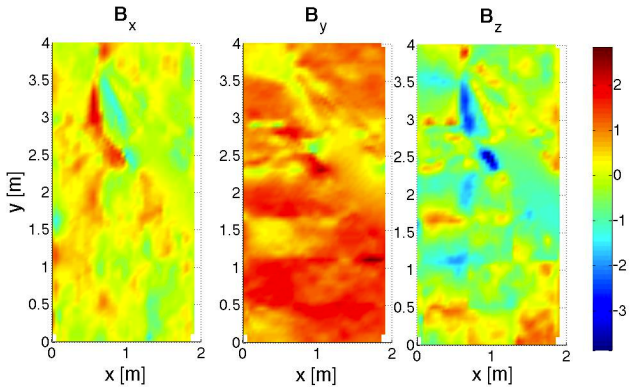

Fig. 22. Two-dimensional map of all three magnetic field components obtained with the omnidirectional ground robot.

While we had expected to see a more regular structure, we consider the unexpected irregular structure of the field to be beneficial for localization purposes. We expect that due to the lack of regularity, any two sequences of measurements taken during even short trajectories, should be so distinguishable that ambiguities are quickly resolved.

V. Conclusions and Outlook

We have shown that the magnetic field in indoor environments is strongly modulated in space and measurable with very little noise. We have also shown that the use of all three field components provides good resolution of ambiguities. We have demonstrated for a 1D-case that even single samples of the field allow to resolve the location with sub-centimeter accuracy with no ambiguity on a segment of length one meter. In one of our next steps we plan to investigate to what degree ambiguities in the magnetic field exist in wider areas and how long recorded trajectories need to be in order to resolve them with high probability.

It has become clear that the stronger the magnetic field is perturbed, the better we may be able to use it for localization purposes. We recognize that this is in contrast to common intuition. Moreover, we predict that – given an accurate map of the magnetic field – centimeter- or sub-centimeter accuracy of location determination should be achievable in indoor environments with today's state of the art MEMS-based inertial and magnetic sensor packages. We further predict that if this accuracy is achievable with distinct mapping and localization phases, simultaneous localization and mapping (SLAM) will converge and achieve the same accuracy, be it with sensors carried on human feet or on ground robots.

While this hints significant potential for the use of the magnetic field for indoor navigation, a number of interlinked questions with practical relevance, such as how achievable accuracy and convergence for both localization and SLAM depend on the resolution of the magnetic maps, sensor noise and possible temporal changes of the field need to be addressed in future work.

References

[1] J. Leonard and H. Durrant-Whyte, "Simultaneous map building and localization for an autonomous mobile robot," in *Proceedings of the IEEE Int. Workshop Intell. Robots Syst. (IROS), Osaka, Japan, 1991*, vol. 3, Nov 1991, pp. 1442–1447.

[2] E. Foxlin, "Pedestrian tracking with shoe-mounted inertial sensors," *IEEE Computer Graphics and Applications*, vol. 25, no. 6, pp. 38–46, Nov. 2005.

[3] P. Bahl and V. N. Padmanabhan, "RADAR: An in-building RF-based user location and tracking system," in *Proc. of IEEE Infocom*, 2000, pp. 572 –577.

[4] P. Robertson, M. Garcia Puyol, and M. Angermann, "Collaborative pedestrian mapping of buildings using inertial sensors and FootSLAM," in *Proceedings of ION GNSS, 2011*, September 2011, pp. 1366–1377.

[5] M. Angermann and P. Robertson, "Footslam: Pedestrian simultaneous localization and mapping without exteroceptive sensors - hitchhiking on human perception and cognition," *Proceedings of the IEEE*, vol. 100, no. Special Centennial Issue, pp. 1840 –1848, 13 2012.

[6] J. Bird and D. Arden, "Indoor navigation with foot-mounted strapdown inertial navigation and magnetic sensors [emerging opportunities for localization and tracking]," *Wireless Communications, IEEE*, vol. 18, no. 2, pp. 28 –35, april 2011.

[7] M. Afzal, V. Renaudin, and G. Lachapelle, "Magnetic field based heading estimation for pedestrian navigation environments," in *Indoor Positioning and Indoor Navigation (IPIN), 2011 International Conference on*, sept. 2011, pp. 1 –10.

[8] B. Gozick, K. Subbu, R. Dantu, and T. Maeshiro, "Magnetic maps for indoor navigation," *Instrumentation and Measurement, IEEE Transactions on*, vol. 60, no. 12, pp. 3883 –3891, dec. 2011.

[9] W. Storms, J. Shockley, and J. Raquet, "Magnetic field navigation in an indoor environment," in *Ubiquitous Positioning Indoor Navigation and Location Based Service (UPINLBS), 2010*, oct. 2010, pp. 1 –10.

[10] T. Riehle, S. Anderson, P. Lichter, J. Condon, S. Sheikh, and D. Hedin, "Indoor waypoint navigation via magnetic anomalies," in *Engineering in Medicine and Biology Society,EMBC, 2011 Annual International Conference of the IEEE*, 30 2011-sept. 3 2011, pp. 5315 –5318.

[11] I. Vallivaara, J. Haverinen, A. Kemppainen, and J. Roning, "Simultaneous localization and mapping using ambient magnetic field," in *Multisensor Fusion and Integration for Intelligent Systems (MFI), 2010 IEEE Conference on*, sept. 2010, pp. 14 –19.

[12] ——, "Magnetic field-based slam method for solving the localization problem in mobile robot floor-cleaning task," in *Advanced Robotics (ICAR), 2011 15th International Conference on*, june 2011, pp. 198 –203.

[13] K. Yamazaki, K. Kato, K. Ono, H. Saegusa, K. Tokunaga, Y. Iida, S. Yamamoto, K. Ashiho, K. Fujiwara, and N. Takahashi, "Analysis of magnetic disturbance due to buildings," *Magnetics, IEEE Transactions on*, vol. 39, no. 5, pp. 3226 – 3228, sept. 2003.

[14] Munich Earth Observatory, "Monthly Magnetograms," http://www.geophysik.uni-muenchen.de/observatory/geomagnetism/monthly-magnetograms, 2012.